Hindawi
Geofluids
Volume 2021, Article ID 6678966, 17 pages
https://doi.org/10.1155/2021/6678966

Research Article

Freezing Pressurized Water into a Standard Cylindrical Ice Sample in a Triaxial Cell

Baosheng Wang,[1] **Peixin Sun**,[1] **Tingting Luo**,[1,2] **Tao Zhang**,[1] **and Weihao Yang**[1,2]

[1]*State Key Laboratory for Geomechanics and Deep Underground Engineering, China University of Mining and Technology, Xuzhou, Jiangsu, China*
[2]*School of Mechanics and Civil Engineering, China University of Mining and Technology, Xuzhou, Jiangsu, China*

Correspondence should be addressed to Weihao Yang; whyang@cumt.edu.cn

Received 27 October 2020; Revised 19 November 2020; Accepted 7 April 2021; Published 23 April 2021

Academic Editor: Chun Zhu

The mechanical characteristics of high-pressure frozen ice are a basis for the design of deep underground frozen walls, the drilling of thick permafrost and ice sheets, and the probing of extraterrestrial ice. The continuous control of the sample stress state from freezing to testing is essential for the experimental study of in situ mechanical response of high-pressure frozen ice. In the context, we developed a preparation technique for freezing pressurized water into a standard cylindrical ice sample in a triaxial cell. Through theoretical analysis, a cylindrical water sample with precise dimensions and strong sealing was fabricated using heat shrinkable tubing, sectional end caps, and an assembly cylinder. A mounting device was designed to insert the water sample into the triaxial cell without deformation. In order to deal with the lateral surface irregular of the resulting ice sample caused by freezing expansion, we proposed a pressurization method in which the volume of the confining medium is controlled to restrict the radial deformation of the sample, and the axial pressure on the sample is kept constant; thus, the freezing expansion will develop along the height direction through releasing the expansion pressure. Based on the analysis of sample deformation and finite element numerical simulations, the control method of the temperature fields of the sample and the confining medium was obtained, and the standard cylindrical ice sample which satisfies the geometric accuracy requirements was produced. The comparison of ice samples frozen by different freezing methods showed that the control of the confining medium mean temperature and the sample unidirectional freezing is necessary to improve the dimensional precision of the ice sample.

1. Introduction

As the underground resource exploitation goes deeper, engineering disasters have become increasingly prominent in unstable aquifers [1–6], and the artificial ground freezing is the primary sinking method in such thick stratum [7]. The frozen depths of alluviums and aqueous strata have reached 750 m [8] and 950 m [9], respectively. However, due to the inadequate understanding of the formation mechanism of frozen soil and frozen rock in deep underground, the static [10] and dynamic [11] responses of deep frozen wall measured in the field are obviously different from the theoretical expectation. The depth of the permafrost in the Arctic can exceed one kilometer [12], but the deep permafrost is difficult to be drilled and sampled [13], which restricts the process of related scientific investigation. To solve these problems, the mechanics experiments of deep frozen soil [14–16] and frozen rock [17–19] have been widely studied, whereas little attention has been paid to the coupling problems of ice-soil and ice-rock and the mechanical characteristics of the ice in deep environment are the basis of the above problems. Compared with the shallow layer conditions, the formation pressure of deep underground surges dramatically; coupled with the ground restrictions imposed on frost heave, the freezing pressure of deep underground water may be above 10 MPa. The influence of such high freezing pressure on the mechanical characteristics of the ice needs to be further studied.

Lake Vostok in Antarctica lies beneath a 4 km thick ice sheet [20]. The lake water is of great scientific value as it has existed for a quite long history and was completely isolated from the outside world. At the beginning of this century, a Russian scientific investigation team started drilling the thick ice sheet to sample the lake water. However, before drilling through the bottom of the ice sheet, the unexpected accident that the lake water suddenly gushes into the drill hole has occurred many times, resulting in poor sampling qualities [21]. Isotope studies showed that over 200 m thick of bottom ice was frozen by high-pressure lake water [22]; thus, revealing the mechanical characteristics of high-pressure frozen ice can promote the drilling and sampling technology of thick ice sheet. Beside, high-pressure water icing also exists in extraterrestrial aqueous environments. For instance, the liquid water of Europa is stored beneath an ice layer of approximately 150 km in thickness, and a substantial part of basal ice was accreted by high-pressure water [23]. As the observation of ice shell rheology is one of the principal means to explore the extraterrestrial liquid water resources, whether freezing pressure affects the rheological characteristics of ice is worth to be studied.

The control of the sample stress state in the processes of sample preparation and experiment is a key technique of the experimental study of high-pressure frozen ice. At present, the preparation technique of ice sample mainly includes three steps, first freezing water (from the top down) into large-scale ice mass in a tank, then the ice samples need to be drilled, cut, and ground to the standard shape, and finally the ice samples are transferred from the preparation apparatus into the test equipment [24–26]. Although this preparation technique can apply freezing pressure by adding a hydraulic system to the tank, it is still inaccessible to the control of the sample stress state during freezing. In addition, in the processes of sample shaping and transfer, the stress state of the ice sample cannot be controlled, and some negative stress paths will inevitably be produced, such as the sudden relief of freezing pressure. These stress paths may cause stress concentrations, microcracks, and other defects in the ice sample [27], leading to inaccurate testing results, meaning that the effect of the freezing pressure cannot be fully reflected. Accordingly, a preparation technique that enables continuous control of the sample stress state from freezing to testing is required to carry out suitable mechanical experiments on ice frozen under high pressure.

To address the challenges above, we proposed a process that consists of first preparing a cylindrical water sample, then pressurizing the water sample in a triaxial cell, and finally freezing it into a standard cylindrical ice sample under stable pressure. After freezing is complete, the stress state of the ice sample can be transitioned from the freezing pressure state to the test conditions in a controllable way. Because of the flexible side constraints of such a cylindrical sample, the sample lateral surface is easy to be irregular during the fabrication and insertion of a water sample and the freezing process. Hence, it is necessary to conceive a technique for shaping and sealing a water sample and then conduct the study of the pressuring and freezing techniques.

2. Ice Sample Size and Precision Standards

The size range of the cylindrical ice samples used in ice mechanics experiments is wide; the diameters range between 18 mm and 100 mm, and the heights range from 40 mm to 260 mm [28–33]. According to the research of Kuehn et al. [34], the results of mechanical tests of ice samples are nearly independent of the sample size when the ratio of height to diameter is fixed. Related studies [35–37] have indicated that within the range of height/diameter ratios of 2–2.5, the radial constraints at the end planes can be neglected. Hence, we chose to prepare an ice sample of 61.8 mm in diameter and 125 mm in height, which is a standard sample size for mechanical tests of frozen soil.

The proposed preparation technique involves freezing the water sample under soft lateral constraints. Due to freezing expansion, the lateral surface of the resulting ice sample is easy to be irregular. However, neither previous ice sample preparation techniques [26, 38] nor ice mechanical test standards [39] have specifically mentioned the geometric tolerances of the samples. Because the accuracy in the radial dimension directly influences the test results, we therefore employed sample dimension tolerances from rock test standards [40], which specify that the lateral surface of a cylindrical sample should be straight to within 0.5 mm over the full height. In addition, the relative error between the average diameter and the design value should be no more than 0.5% to limit the error on the cross-sectional area of the cylinder to less than 1%. Accordingly, the average diameter of our ice sample should be within 61.8 ± 0.3 mm. The height error of the sample has no obvious effect on the test results, but considering the requirements on the height/diameter ratio, the ice sample height should be within 125 ± 1mm.

3. Preparation of a Cylindrical Water Sample

The first procedure of the preparation technique is to produce a cylindrical water sample. Unlike solid materials, liquids have no definite shape; therefore, the geometry of a water sample must be formed and maintained by its packaging. Thus, we planned to fabricate a cylindrical package with a soft flank and then inject water into it. Water expands by 9% in volume when frozen to ice Ih [41], and the preparation technique would force the freezing expansion to develop along the height direction. Hence, the ratio of the ice sample height to the water sample height will be 1.09, and the desired water sample dimensions are therefore 61.8 mm in diameter and 114.7 mm in height.

3.1. Flexible Membrane. The cylindrical sample to be pressurized in the triaxial cell should be centred between two rigid end caps and wrapped in a flexible tubular membrane to prevent the confining medium from coming into direct contact with the experimental material. Our novel preparation technique also requires the membrane to maintain the geometry of the water sample. This means that the perfect membrane should not only possess sufficient stiffness and thickness to resist the initial internal water pressure and prevent the water sample from bulging beyond its limit but also be soft enough

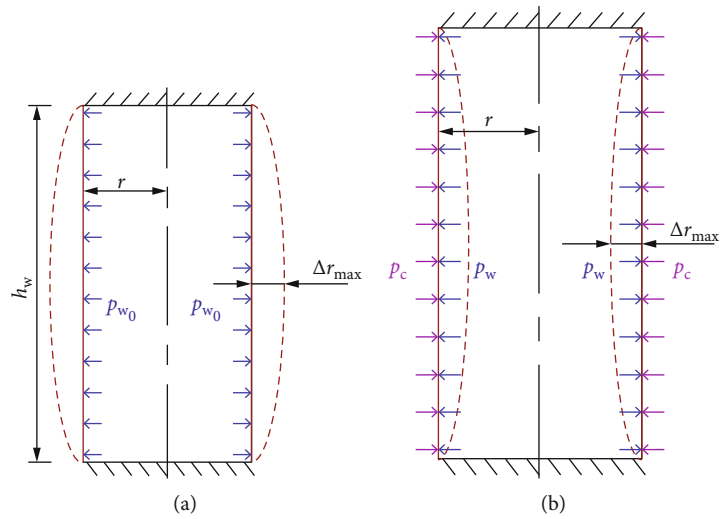

FIGURE 1: Mechanical models of the flexible tubular membrane: (a) bulging due to the initial internal water pressure and (b) compressed by confining pressure.

that the confining pressure can be transmitted without reduction. Because the deformation resistance of the membrane is much weaker than that of the end caps (steel), the mechanical model of the tubular membrane can be simplified as a thin-walled cylindrical shell with fixed ends (Figure 1). It is difficult to solve this model under a linearly varying radial pressure, which is the actual distribution of the initial internal water pressure. We therefore assume that the maximum water pressure is equally distributed inside the sample to estimate the bulging deformation (Figure 1(a)), such that the initial internal water pressure is $p_{w0} = \gamma_w h_w$, where γ_w is the specific gravity of water and h_w is the height of the water sample. The maximum radial displacement of the model, Δr_{max}, under a uniform pressure p can be calculated as [42]

$$\Delta r_{max} = \frac{pr^2}{Et}, \tag{1}$$

where r, E, and t are the radius, elastic modulus, and thickness, respectively, of the membrane. On the basis of the geometric tolerance of the ice sample, Δr_{max} should be no greater than 0.25 mm. Substituting $p = p_{w0}$ into equation (1), we obtain $Et \geq 4.4$ MPa mm. The typical membrane materials used in triaxial tests of ice, frozen soil, and rock are separately indium [43], rubber [44], and heat shrinkable tubing [45, 46]. Among them, indium is expensive, complicated to form into a thin cylinder, and with low radioactivity. The elastic modulus and thickness of a typical rubber jacket are approximately 6 MPa and 0.5 mm, respectively, which means that such a jacket would allow our water sample to bulge past its limit. By contrast, PVC heat shrinkable tubing has an elastic modulus of approximately 150 MPa and a thickness of 0.4 mm after shrinkage, allowing it to maintain the dimensions of the water sample. The mechanical model of the water sample compressed by confining pressure p_c is shown in Figure 1(b), where p_w is the internal water pressure. Under these circumstances, the radial deformation should remain within the geometric tolerance. By substituting $\Delta r_{max} \leq 0.25$ mm, $p = p_c - p_w$, and the E and t values of the heat shrinkable tubing into equation (1), $p_c - p_w \leq 0.016$ MPa is obtained. This difference is far less than the planned confining pressure (at least 10 MPa), meaning that p_c is approximately equal to p_w and the transmission rate for the confining pressure is close to a hundred percent. Therefore, we selected heat shrinkable tubing as the flexible membrane.

3.2. Fabrication of the Cylindrical Water Sample. Two problems needed to be solved for the fabrication of the cylindrical water sample. One was that a cylindrical supporting structure must initially be centred between the two end caps to support the shrunken size of the heat shrinkable tubing, and it must be able to be removed after shrinkage. The other was that the sealing between the heat shrinkable tubing and the end caps should prevent not only the inflow of the confining medium but also outward seepage of the water, which cannot be achieved through the traditional method of arranging sealing rings on the sides of the end caps. To address these problems, we developed the sample package fabrication process depicted in Figure 2. One of the two end caps was divided into an outer cap and an inner cap with a threaded connection. A water injection hole equipped with a closure bolt was introduced into the other end cap on the central axis. An assembly cylinder consisting of an inner location column and an outer split tube was machined. The location column consists of two concentric sections: a long section whose diameter is equal to the inside diameter of the outer cap and a short section with the same diameter as the water injection hole. The split tube is divided into four pieces along the circumferential direction, with the same external dimensions and internal diameter as the water sample and the outer cap, respectively. During the fabrication process, first, the outer cap and the end cap are separately placed around the ends of the location column, and the split tube is fitted together around the outside to compose the assembly cylinder (Figure 2(a)). Note that the split tube must be in direct

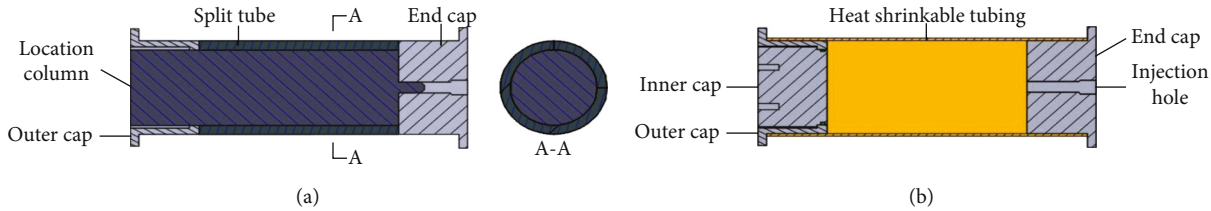

Figure 2: Fabrication process for the water sample package, including (a) the composition of the assembly cylinder and (b) the completed state of the water sample package.

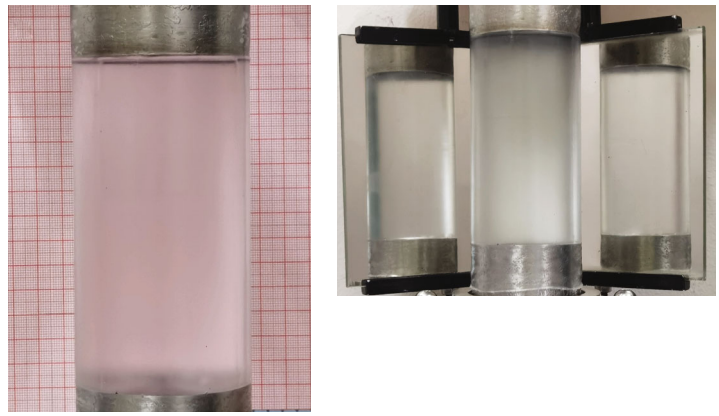

Figure 3: The fabricated water sample: (a) the side lengths of a big square and a small one in the grid is 1 cm and 1 mm, respectively, and (b) the included angle of the mirrors is 120°.

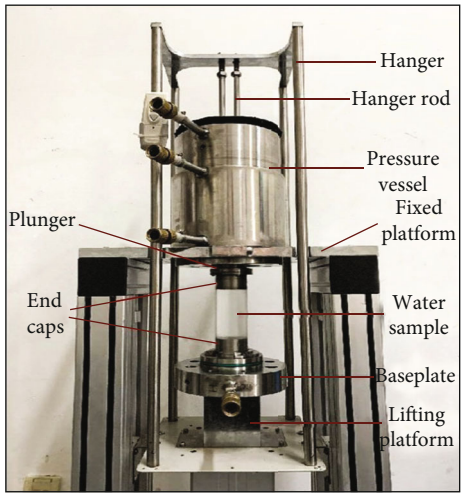

Figure 4: Mounting device.

contact with the two caps. Then, a type of flexible adhesive with low-temperature resistance and a slow curing speed is daubed onto the sides of the caps. Heat shrinkable tubing is placed around the whole structure and heated to tightly wrap the caps and split tube. After the adhesive is fully cured, the location column and the split tube are removed in turn through the outer cap. Finally, by fastening the inner cap to the outer cap, the water sample package is completed (Figure 2(b)). After filling the package with degassed distilled water through the water injection hole and then tightening the closure bolt, the final cylindrical water sample is obtained.

Table 1: Physical properties of three commonly used low-temperature hydraulic fluids, as provided by the manufacturers.

	Pour point (°C)	Bulk modulus (GPa)	Volume thermal expansion (°C)
Low-temperature hydraulic oil	-35	1.6	7.8×10^{-4}
Dimethyl silicone oil	-60	1.1	9.9×10^{-4}
Aviation hydraulic oil	-65	1.4	9.8×10^{-4}

Figure 3 shows that the lateral surface of the fabricated water sample is quite straight.

3.3. Insertion of the Water Sample. As the water sample has no deformation resistance to bear the gravity of the end cap and the plunger, measures should be taken to maintain the relative positions of the upper and lower ends of the water sample invariant during the insertion process. For this reason, we designed a mounting device shown in Figure 4, which mainly consists of a fixed platform and a lifting platform. The pressure vessel is clamped at the centre of the fixed platform. The lifting platform is equipped with a hanger and two hanger rods. The plunger is suspended inside the pressure vessel by the hanger rods, and the baseplate is placed on the lifting platform. The central axes of the plunger, the pressure vessel, and the baseplate are aligned. During the insertion of a water sample, its upper and lower end caps are fastened to the

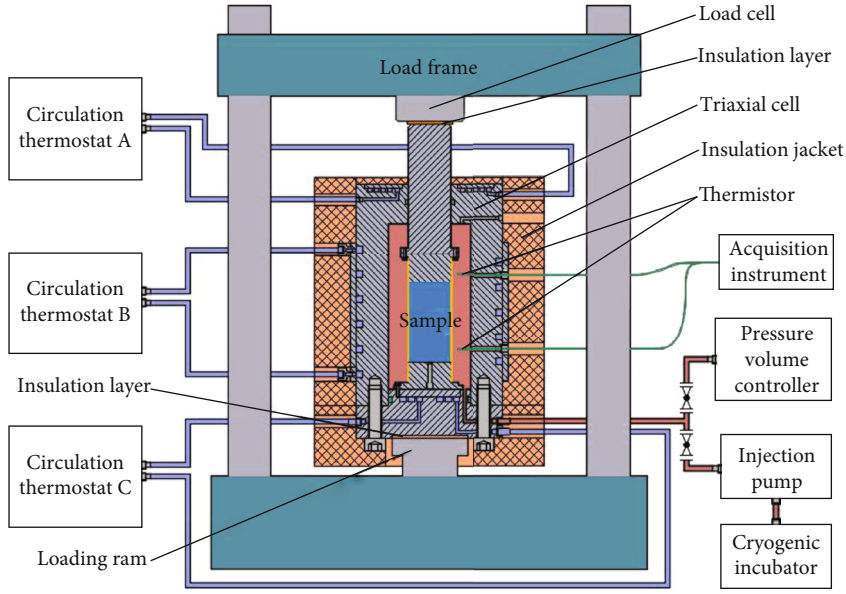

Figure 5: Schematic diagram of the KTL-401 servo-controlled low-temperature triaxial testing system.

plunger and the baseplate, respectively. Then, the lifting platform synchronously raises the plunger and the baseplate. As a result, the water sample is inserted without deformation.

4. Pressurization Method

4.1. Apparatus. The water sample is pressurized and frozen by a KTL-401 servo-controlled low-temperature triaxial testing system, which is codeveloped by China University of Mining and Technology and KTL Instruments Company. It is capable of imposing an axial load of up to 400 kN and the confining pressure of up to 64 MPa with an accuracy of 0.05%. The triaxial cell is cooled by circulating refrigerant from three circulation thermostats, A, B and C, passing through the upper, lateral, and lower freezing channels of the cell, respectively. The triaxial cell temperature is controlled by regulating the temperature of the circulation thermostats (adjustable down to -60°C in increments of ±0.1°C). A 60 mm thick insulation jacket is wrapped around the cell to prevent excessive inward heat flow from the surroundings, and two 1 mm thick insulation layers are placed at the top and bottom of the cell to reduce the cooling energy loss to the load frame. The internal temperature of the triaxial cell is measured by two thermistors with a resolution of 0.01°C, which are threaded through the lateral wall and connected to an acquisition instrument.

4.2. Confining Medium Injection and Pressurization. The choice of confining medium was dictated by the requirements that the medium should remain fluid at low temperature and its volume should be little influenced by changes in temperature and pressure. Three commonly used low-temperature hydraulic fluids were compared (Table 1). Because of its high pour point, low-temperature hydraulic oil loses fluidity below -35°C; therefore, it is difficult to be injected and inappropriate for pressure conduction at such low temperatures. Between the other two fluids, we chose aviation hydraulic oil as the confining medium because its compressibility and thermal expansion are lower than those of dimethyl silicone oil.

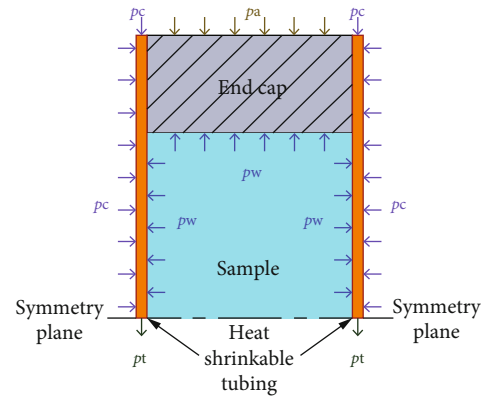

Figure 6: Mechanical model of the water sample under stable pressure.

Before the pressurization process, the aviation hydraulic oil is first subjected to a vacuum of -0.1 MPa for 24 h to remove air bubbles; then, it is sealed and stored in a cryogenic incubator for at least 24 h to be cooled to a sufficiently low temperature. After that, the oil is injected by an injection pump whose inlet and outlet pipes are connected to the cryogenic incubator and the triaxial cell, respectively (Figure 5). The injection pump and the connecting pipes are insulated to maintain the temperature of the oil during injection. Once the injection process is completed, within approximately 30 s, the water sample is pressurized to a given pressure at a speed of 0.2 MPa s^{-1} by a pressure volume controller. During oil injection and pressurization, the height of the water sample is kept constant by the load frame.

4.3. Pressure Stabilization. After the pressure of the water sample reaches the given value, the water sample must be

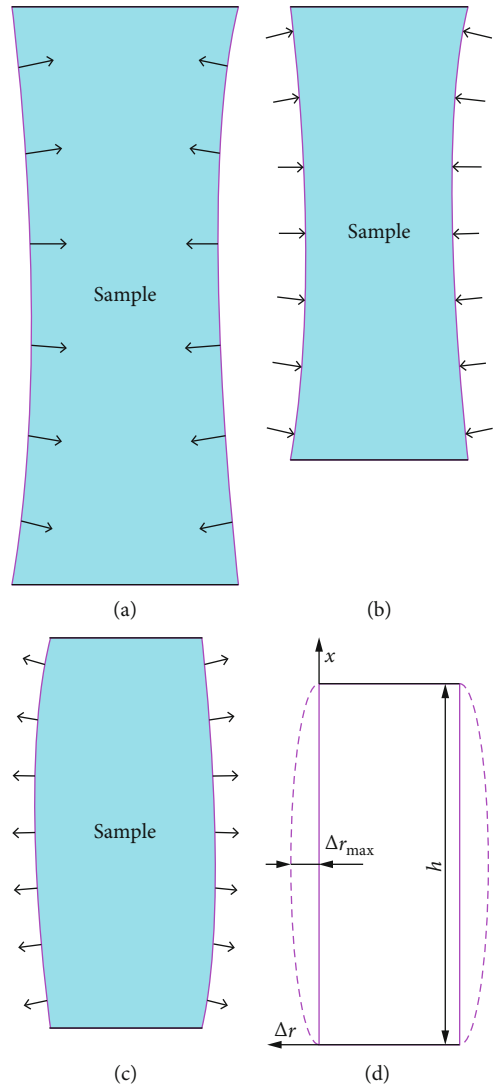

Figure 7: Radial deformation of the sample caused by (a) water cooling, (b) water compression, and (c) the thermal volume change of the confining medium and (d) the deformation model.

frozen under stable pressure. To force the freezing expansion to develop along the height direction of the sample, the quantity of the confining medium in the triaxial cell is locked by the pressure volume controller, and the sample pressure is then controlled by the load frame, which is set to apply a constant axial pressure. When freezing expansion occurs, the radial deformation of the sample is restricted by the stable volume of the confining medium, and the freezing expansion develops along the height direction as the expansion pressure releases.

The mechanical model of the water sample under stable pressure is shown in Figure 6. Along the height direction, the axial pressure p_a applied by the load frame, the tensile stress of heat shrinkable tubing p_t produced by the extension of the sample, the confining pressure p_c, and the internal water pressure p_w have the following relation:

$$p_a A_a + p_c A_t + p_t A_t = p_w A_a, \tag{2}$$

where A_a and A_t are the cross-sectional areas of the end cap and the heat shrinkable tubing, respectively, and can be easily calculated from the dimensions of the water sample package. According to the mechanical analysis of the heat shrinkable tubing presented in Section 3.1, $p_c = p_w$ was obtained in the radial direction of the sample. Thus, equation (2) is converted into

$$p_c = 1.03p_a + 0.027p_t. \tag{3}$$

The material used as the heat shrinkable tubing is a kind of PVC film. Uniaxial tensile tests [47, 48] have indicated that the stress-strain relation of such PVC film is linear in a strain range of 0-20%. Hence, the heat shrinkable tubing exhibits linear deformation during sample extension, that is,

$$p_t = E\frac{\Delta h}{h_w}, \tag{4}$$

where Δh is the increase in the sample height, h_w is the height of the water sample, and E is the elastic modulus of the PVC heat shrinkable tubing. Substituting equation (4) into (3), we obtain

$$p_c = 1.03p_a + \lambda\Delta h, \tag{5}$$

where $\lambda = 0.035$ MPa/mm. We can see that p_c is slightly greater than p_a. Because p_a is constant controlled by the load frame, p_c increases linearly with Δh by a gradient of 0.035 MPa/mm. Ideally, the sample should extend 10.3 mm in the height direction due to freezing expansion; thus, the total increment in p_c during freezing will be approximately 0.36 MPa.

5. Freezing Technique

Given the pressurization method described above, the freezing technique should satisfy the following three requirements:

(1) Although the quantity of the confining medium in the triaxial cell is locked by the pressure volume controller, the volume of the confining medium still depends on its temperature. Hence, the mean temperature of the confining medium should be controlled in order to control its volume

(2) The freezing form of the sample should be unidirectional (along the central axis)

(3) The whole sample freezing process should occur under stable pressure, which means that the sample should not begin to freeze before the completion of pressurization

As the confining medium mean temperature must be below the melting point of water when the sample is being frozen, the aviation hydraulic oil should be maintained at a stable negative temperature from the injection of the oil to the completion of the sample freezing. To avoid the low-temperature oil being rapidly heated by the hot triaxial cell, we designed an operating procedure in which the triaxial cell is first precooled, and then, the precooled oil is injected and the sample is pressurized, and finally, the sample is frozen under stable pressure.

5.1. Analysis of Sample Radial Deformation. It is impossible to control the mean temperature of the confining medium without any error. To determine the permissible range of variation of the mean temperature, we analysed the radial deformation of the sample during pressurization and freezing, which is mainly caused by the following three phenomena:

(1) The water sample shrinks radially when being cooled (Figure 7(a)), leading to a sample volume reduction ΔV_{wc}, which can be calculated as

$$\Delta V_{wc} = \alpha_w V_w, \tag{6}$$

where V_w is the volume of the water sample and α_w is the ratio of volumetric change of water. The water is cooled from room temperature (20°C) to the melting point. According to the test results of Kell [49], during this cooling process, the water volume first decreases and then increases (the density of water is highest at 4°C), and the total ratio of volumetric change is -1.63×10^{-3}

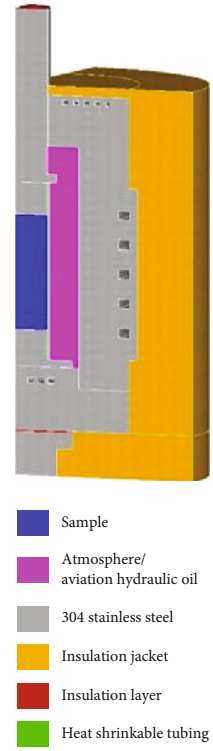

Figure 8: Finite element model of the triaxial cell and its internal components.

(2) The water sample is radially compressed during the pressurization process (Figure 7(b)). According to the results of the analysis presented in Section 3.1, the confining pressure p_c is approximately equal to the internal water pressure p_w; thus, the volumetric compression of the water sample ΔV_{wp} can be expressed as

$$\Delta V_{wp} = -\frac{V_w p_c}{K_w}, \tag{7}$$

where $K_w = 2.2$ GPa is the bulk modulus of water [50]

(3) When the sample is frozen under stable pressure, its radial deformation is controlled by the volume of the confining medium (Figure 7(c)), which varies with the mean temperature of the confining medium. This volume change, ΔV_c, can be calculated as

$$\Delta V_c = \beta_c V_c \Delta T_c, \tag{8}$$

where β_c is the volume thermal expansion coefficient of aviation hydraulic oil (Table 1), $V_c = 2.2 \times 10^6$ m

Table 2: Material parameters of the finite element model. The water and ice parameters were taken from Blue [56], Slack [57], Gu and Stefan [58], and Ramires et al. [59]; the 304 stainless steel parameters were taken from Cubberly et al. [60]; the atmospheric parameters were from Tsilingiris [61]; and the parameters of the other components were provided by the manufacturers.

	Water	Ice	304 stainless steel	Heat shrinkable tubing	Aviation hydraulic oil	Atmosphere	Insulation layer	Insulation jacket
Density ($kg\,m^{-3}$)	1000	920	7930	1400	865	1.293	1500	100
Heat capacity ($kJ\,kg^{-1}°C^{-1}$)	4200	2100	500	1200	2100	1004	1400	2250
Thermal conductivity ($W\,m^{-1}°C^{-1}$)	0.58	2.3	15	0.2	0.15	0.025	0.15	0.05

m^3 is the initial volume of the confining medium in the triaxial cell, and ΔT_c is the change in the mean temperature of the confining medium

To comprehensively consider the above three factors, we established a deformation model of the sample, which is shown in Figure 7(d). The relation between the volume changes caused by these three factors and the radial deformation of the sample is

$$\Delta V_{wc} + \Delta V_{wp} + \Delta V_c = \int_0^h \left[\pi(r + \Delta r)^2 - \pi r^2\right] dx, \quad (9)$$

where r is the sample radius. According to the analytical calculations of Huang et al. [51], the deflection of the model can be approximated as a sinusoidal curve, that is,

$$\Delta r = \Delta r_{max} \sin\left(\frac{x\pi}{h}\right). \quad (10)$$

The radial deformation of the sample should not exceed the geometric tolerance. By substituting $|\Delta r_{max}| \leq 0.25$ mm into equations (6)–(9), the permissible variation range of the confining medium mean temperature can be simultaneously determined:

$$\Delta T_c \in [-2.1 - 0.073p_c, 1.6 - 0.073p_c]^\circ C, \quad (11)$$

where the unit of p_c is MPa. The permissible variation range can also be expressed as $[(-0.25 - 0.073\,p_c) \pm 1.85]^\circ C$. This means that once the sample begins to freeze, the volume of the confining medium should be slightly decreased by changing the mean temperature by $(-0.25 - 0.073\,p_c)^\circ C$ to allow the freezing expansion to develop to a small extent along the radial direction to compensate for the small radial shrinkage of the water sample caused by cooling and compression, then the mean temperature of the confining medium should remain constant until the sample is completely frozen, and the permissible fluctuation of above temperature control is ±1.85°C.

5.2. Finite Element Model. The essence of the freezing technique is to control the temperature field developments of the sample and the confining medium, and its basic requirement is to know the real-time status and variation trend of the temperature field. However, the KTL-401 system has only two temperature measurement points, which are unable to provide the necessary temperature data. Therefore, we used numerical simulations to indirectly acquire information on the temperature in the triaxial cell. A finite element model of the triaxial cell and its internal components was built in the ANSYS software (Figure 8). In this model, all components have the same dimensions as in the actual condition except the sample, which has a fixed size equal to that of the ice sample, meaning that freezing expansion is neglected. The material parameters of the model components are shown in Table 2. According to the conclusions of Makita [52] and Otero et al. [53], the material parameters of water and ice change little within the temperature and pressure ranges of the KTL-401 system, so they are taken to be equal to their values under standard atmospheric pressure. The latent heat of water freezing is $335\,kJ\,kg^{-1}$ [54], but because of the neglect of freezing expansion, the latent heat of the modelled sample is taken to be equal to that of water divided by 1.09, which is $307.3\,kJ\,kg^{-1}$. The freezing temperature of water, T_f, is affected by pressure and can be obtained through the iterative solution of the accurate regression formula reported by Wagner et al. [55]:

$$1 - 0.626000 \times 10^6 \times \left[1 - \left(\frac{T_f}{T_n}\right)^{-3}\right] + 0.197135 \times 10^6 \times \left[1 - \left(\frac{T_f}{T_n}\right)^{21.2}\right] = \frac{p_f}{p_n}, \quad (12)$$

where $T_n = 273.16$ K, P_f is the freezing pressure, and $P_n = 0.000611657$ MPa. The side of the model is in direct contact with the air, so the boundary conditions at these surfaces correspond to convective heat transfer. Because the top and bottom of the triaxial cell are engaged with the metallic loading frame, which is directly exposed to air, the temperatures of these two surfaces are assumed to be constant. To determine the boundary parameters, a pressurized freezing operation was implemented by circulating refrigerant at a constant temperature of -25°C in the lateral freezing channel to precool the triaxial cell for 30 min and then freeze the sample under 20 MPa with an initial oil temperature of -15°C, and the measured temperature changes were recorded. Then, a numerical simulation of the temperature field during the above operation was carried out. The initial temperature of the model in the simulation was set equal to the actual ambient temperature of 20°C. The freezing temperature of the sample was determined by iteratively solving equation (12)

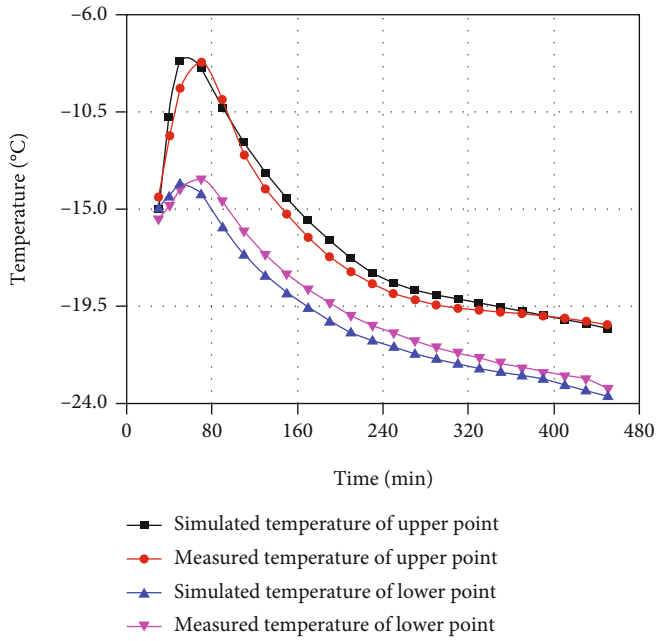

Figure 9: Simulated and measured temperature changes at the two measurement points.

and was found to be -1.53°C. In the simulation of the precooling of the triaxial cell, atmospheric properties (Table 2) were assigned to the elements in the region of the confining medium. Considering that the oil injection and pressurization process takes only 3 min, this process was simplified as instantaneous in the simulation. Once the oil was injected, the properties of these elements were replaced with the material parameters of the aviation hydraulic oil (Table 2), and the instantaneous temperature of the corresponding nodes was modified to the initial oil temperature. The boundary parameters were adjusted to cause the simulated temperature change at the measurement locations close to the measurement results, and the definitive parameters were as follows: the temperature and heat convection coefficient at the sides of the model were 20°C and 25 W $m^{-2}°C^{-1}$, respectively, and the temperatures at the top and bottom of the model were 8°C and 13°C, respectively. The simulated and measured temperatures at the two measurement points are shown in Figure 9. Because of both the neglect of the change in the sample size and the simplification of the oil injection and pressurization process, which mainly affected the accuracy of the simulation in the early stage, the differences between the simulated and measured results prior to 240 min are obviously larger than the differences after that time, and the maximum and minimum differences are 1.25°C and 0.5°C, respectively.

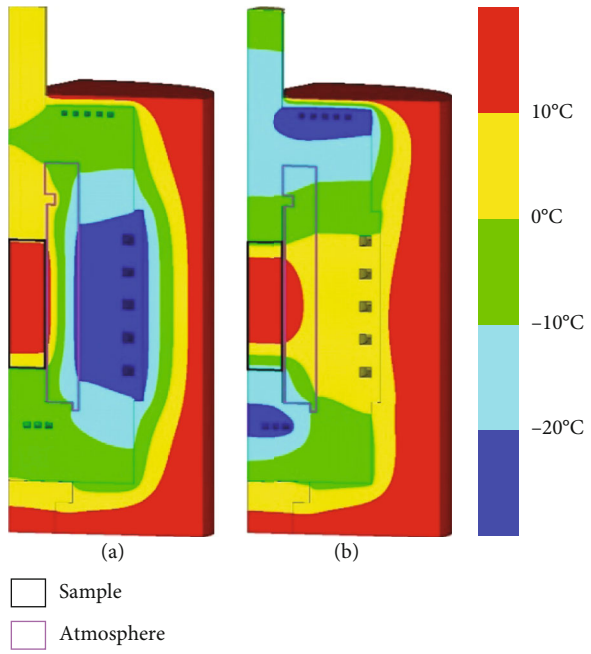

Figure 10: Simulated temperature fields in the finite element model under cooling by (a) the lateral freezing channel and (b) the upper and lower freezing channels with a constant temperature constraint of -25°C for 40 min.

5.3. Freezing Method. Two problems needed to be solved to realize the desired freezing technique. One was to determine which of the three freezing channels in the triaxial cell are most appropriate to use for the precooling of the triaxial cell, oil injection and pressurization, and the freezing of the sample, respectively. The other was to determine how to regulate the temperatures of the three circulation thermostats to control the temperature field developments of the sample and the confining medium to meet the three requirements proposed at the beginning of this chapter.

First, the evolution of the temperature field in the finite element model was simulated under 40 min of cooling with different freezing channels by a constant freezing channel temperature constraint of -25°C. According to the simulation results shown in Figure 10, the cooling energy of the upper

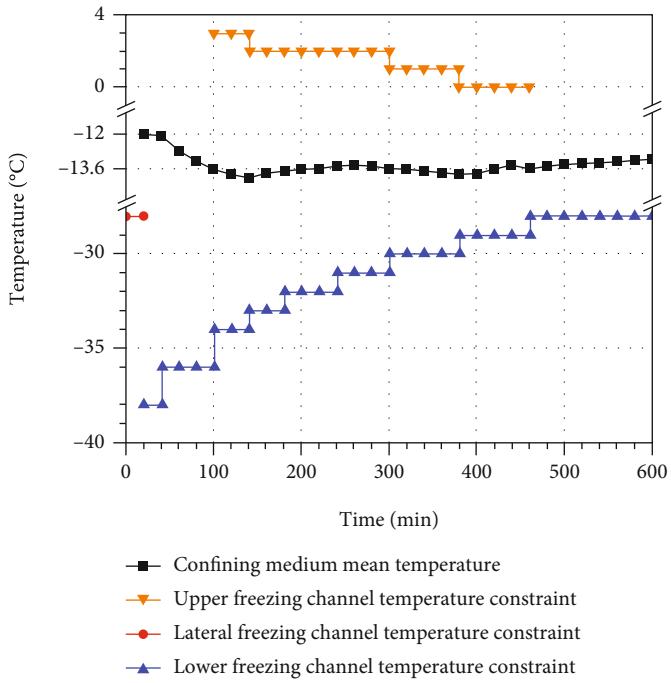

Figure 11: Changes in the adjusted temperature constraints on the three freezing channels and the simulated mean temperature of the confining medium under the conditions that the initial oil temperature is -12°C and the freezing pressure is 20 MPa.

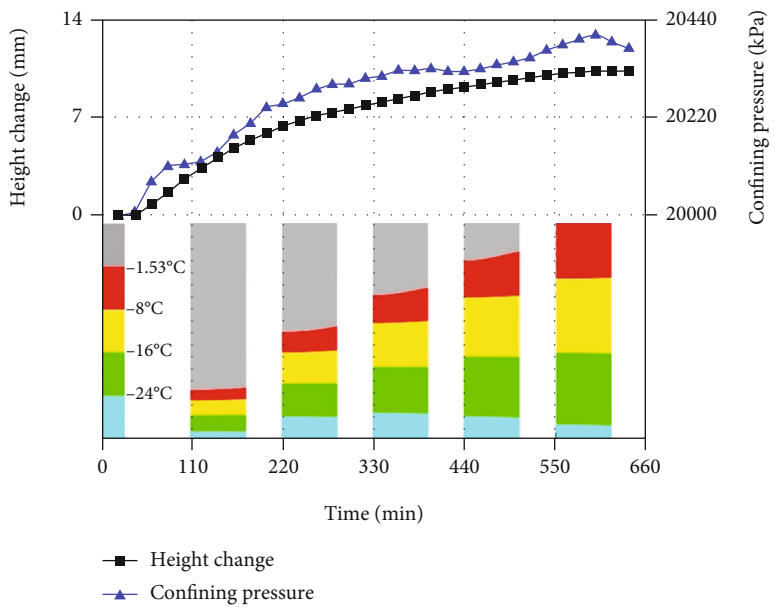

Figure 12: Changes in the simulated freezing state of the sample, the measured sample height, and the measured confining pressure over time by the use of the freezing technique. The freezing state of the sample is shown through an axisymmetric plane, and the time corresponds to the symmetry axis (left border of the plane).

and lower freezing channels can be rapidly transferred to the ends of the sample through the plunger and baseplate, which is suitable for freezing the sample, and the freezing effect of the lower channel is better than that of the upper channel. By contrast, the efficiency of cooling energy transmission from the lateral freezing channel to the ends of the sample is comparatively low because the cooling energy must first pass through the whole triaxial cell, which means that the triaxial cell must be effectively cooled before the sample begins to freeze. Therefore, the lateral freezing channel is more appropriately employed for precooling the triaxial cell as well as during the oil injection and pressurization process, while the upper and lower freezing channels are more suited for freezing the sample.

(a) (b)

Figure 13: Ice sample frozen by the freezing technique: (a) the side lengths of a big square and a small one in the grid are 1 cm and 1 mm, respectively, and (b) the included angle of the mirrors is 120°.

Then, based on this usage of the freezing channels, a satisfactory evolution of the temperature fields of the sample and the confining medium can be simulated by adjusting the temperature constraints of the freezing channels in simulation, and the results of simulated temperature constraints of freezing channels can be used for the regulation of the temperatures of the circulation thermostats during the actual freezing operation. In the simulation, the sample is controlled to freeze in bottom-up direction, which is more efficient than top-down freezing (Figure 10). According to equation (11), the control error of the mean temperature of the confining medium is ±1.85°C. Considering that the maximum difference between the simulated result and the actual measured temperature is 1.25°C (Figure 9), the mean temperature control tolerance in the simulation is reduced to ±0.6°C. In accordance with the actual operating procedures, the simulation was divided into four stages:

(1) The first stage corresponds to the simulation of the processes of triaxial cell precooling and oil injection and pressurization. The temperature constraint on the lateral freezing channel and the precooling time are adjusted to limit the fluctuations in the simulated mean temperature of the oil to less than ±0.6°C during oil injection and pressurization. As mentioned above, the 3 min process of oil injection and pressurization is simplified as being completed instantaneously in the simulation; then, we use the 3 min of time after the activation of the aviation hydraulic oil properties to approximately simulate the development of the temperature field during this period. If the sample begins to freeze in this stage, it indicates that the initial oil temperature is too low, and the simulation should be restarted after properly increasing the oil temperature

(2) After the simulation of oil injection and pressurization, the temperature constraint on the lateral freezing channel is deleted, and the temperature constraints on the upper and lower freezing channels are adjusted to gradually form a gradient temperature field of cold in the lower and hot in the upper in the triaxial cell and maintain the fluctuations of the mean temperature of the oil within ±0.6°C

(3) Once the sample begins to freeze, according to equation (11), the temperature constraints on the upper and lower freezing channels are adjusted to slowly decrease the mean temperature of the oil by $(-0.25 - 0.073\,p_c)$°C

(4) After the mean temperature of the oil decreases by $(-0.25 - 0.073\,p_c)$°C, the temperature constraints on the upper and lower freezing channels are adjusted to stabilize the mean temperature of the oil at its current value and limit the fluctuations to within ±0.6°C until the sample is completely frozen. Meanwhile, the sample should be controlled to freeze in bottom-up direction

6. Preparation Results of Ice Samples

6.1. Use of the Freezing Technique. An ice sample was prepared by the pressurization method and the freezing technique with an initial oil temperature of -12°C and a freezing pressure of 20 MPa. The numerical simulation was firstly adjusted to obtain a satisfactory evolution of the temperature fields of the sample and the confining medium, and the changes in the adjusted temperature constraints on the three freezing channels and the simulated mean temperature of the confining medium are shown in Figure 11. The pressurized

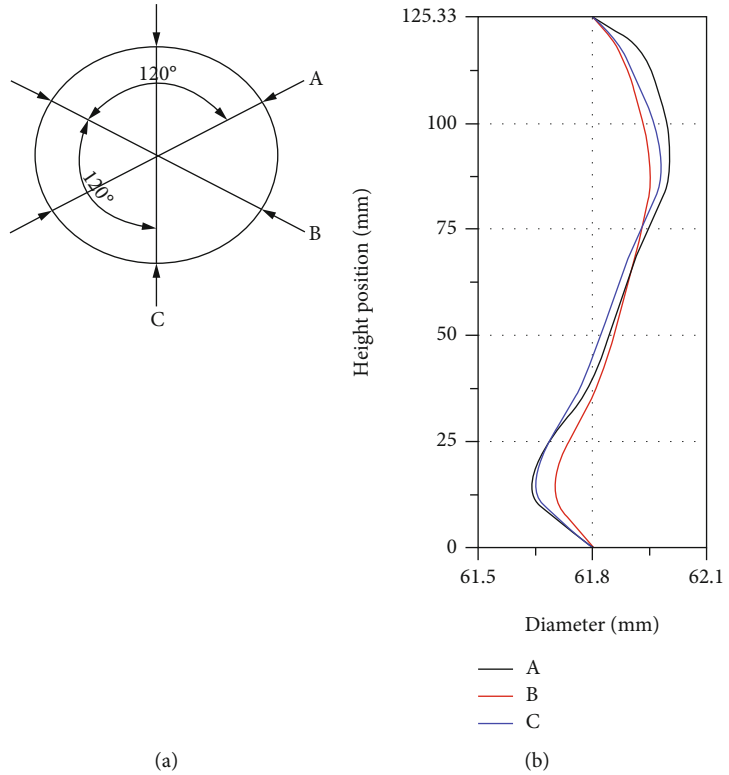

Figure 14: Ice sample diameter: (a) measurement intervals and (b) measurement results.

freezing operation was then performed by regulating the circulation thermostats in accordance with the temperature constraints determined from the simulation. During freezing, as Figure 12 shows, the change in the sample height over time coincided with the development of sample freezing, and the total increase in the sample height was 10.15 mm, which is close to the theoretical value. The confining pressure increased with minor fluctuations, and the increments in the confining pressure and sample height approached the linear relation expressed in equation (5).

After the sample was frozen, the freezing pressure was slowly unloaded by a rate of 0.05 MPa/s with a condition that the axial pressure is equal to the confining pressure. Then, the ice sample was taken out and was observed with no visible irregularities, as shown in Figure 13. The ice sample height was measured to be 125.33 mm (noted that the ice sample height slightly increased during the pressure relief), satisfying the height requirement. The sample diameters were measured along the height direction three times with the same circumferential interval of 120° (Figure 14(a)), and the measurement results are shown in Figure 14(b). The maximum and minimum diameters were 62.01 mm and 61.68 mm, respectively; accordingly, the radial error was 0.33 mm, within the specified dimensional tolerance. The average diameter was 61.92 mm, also within the specified limit.

6.2. Neglect of the Control of the Mean Temperature of the Confining Medium. To verify the necessity of the control of the mean temperature of the confining medium, an ice sample was frozen in bottom-up direction but neglecting the change in the oil temperature, and the initial oil temperature

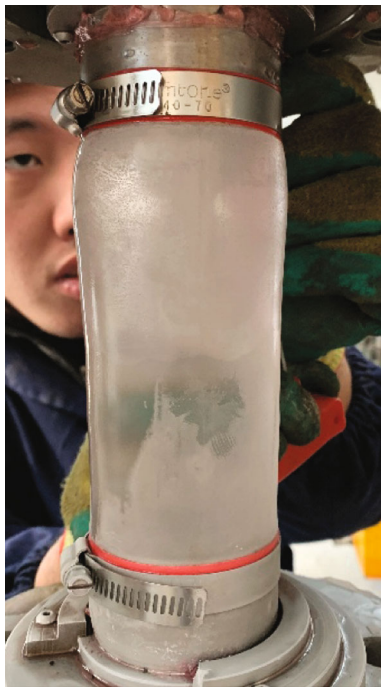

Figure 15: Ice sample frozen in bottom-up direction but neglecting the change in the oil temperature.

and the freezing pressure were also -12°C and 20 MPa, respectively. The operations of triaxial cell precooling and oil injection and pressurization were similar with those in Section 6.1, and then, the sample was frozen in a gradient

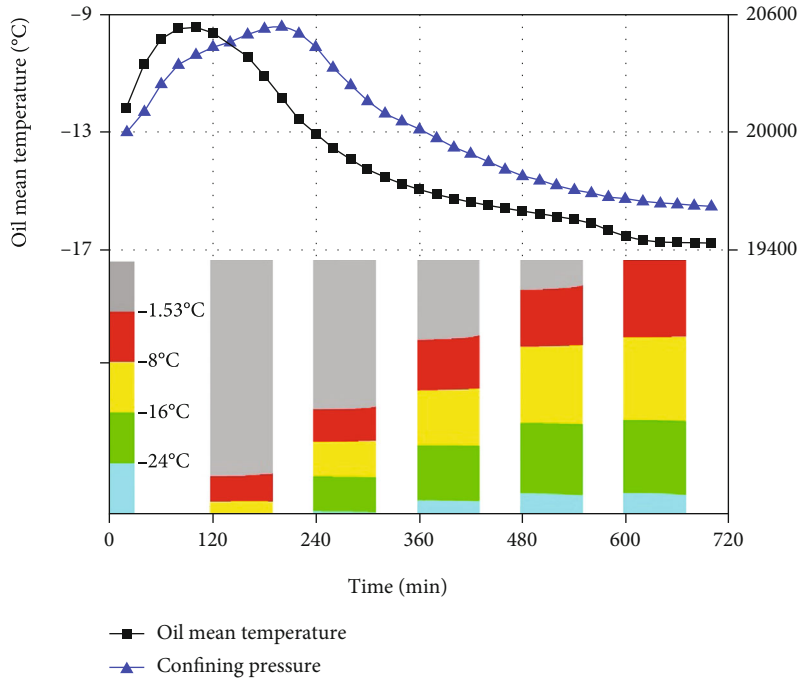

Figure 16: Changes in the simulated freezing state of the sample, the simulated mean temperature of the confining medium, and the measured confining pressure over time under the conditions that the sample was frozen in bottom-up direction but the change in the oil temperature was neglected. The freezing state of the sample is shown through an axisymmetric plane, and the time corresponds to the symmetry axis (left border of the plane).

temperature field which was formed by separately circulating refrigerants of 1°C and -30°C in the upper and lower freezing channels. During freezing, the confining pressure did not monotonically increase, as concluded from the analysis in Section 4.3, but rather initially increased and then decreased, and the total increase in the sample height was only 6.3 mm, which is significantly lower than the theoretical value of 10.3 mm. The resulting ice sample failed to satisfy the geometric tolerance and showed marked swelling on the top half (Figure 15).

To determine the reason for this swelling, the freezing process was analysed through a comprehensive comparison of the changes in the simulated freezing state of the sample, the simulated mean temperature of the confining medium, and the measured confining pressure over time (Figure 16). In the earlier stage of the sample freezing (0–200 min), the freezing rate of the sample was relatively fast, and the mean temperature of the confining medium first increased 2.5°C and then decreased 2.5°C, meaning that the volume of freezing expansion was larger than the volume contraction of the confining medium; consequently, the confining medium was compressed, and the confining pressure rose. After that, the sample freezing was slowing, while the mean temperature of the confining medium steadily dropped, resulting in a reversal of the relationship between the volume of freezing expansion and the volume contraction of the confining medium; thus, the interaction between the sample and the confining medium weakened, and the confining pressure declined. During the whole freezing process, the decrease of the confining medium mean temperature was up to approximately 8°C, more than double the permissible value 3.25°C calculated from equation (11), and most of the temperature decreases occurred in the middle and later period of the freezing. Therefore, the radial expansion of the top half of the sample cannot be properly limited due to the excessive cold contraction of the confining medium. The results of the above analysis confirmed the necessity of controlling the mean temperature of the confining medium.

6.3. Neglect of the Unidirectional Freezing of the Sample. To verify the necessity of the unidirectional freezing, an ice sample was frozen under the condition that the mean temperature of the confining medium was controlled but the sample was frozen with two freezing fronts developing towards each other. The initial oil temperature and the freezing pressure were also -12°C and 20 MPa, respectively. The adjustment simulation was carried out with identical temperature constraints on the upper and lower freezing channels. The pressurized freezing operation was then performed by regulating the circulation thermostats in accordance with the temperature constraints determined from the simulation. During freezing, as shown in Figure 17, the confining pressure slowly rose at a rate close to that indicated by equation (5) until the terminal phase, when it abnormally increased by approximately 1.5 MPa. The total increase in the sample height was 8.9 mm, which is lower than the theoretical value. Most of the radial deformation of the ice sample was restricted except a notable expansion at the middle position (Figure 18).

To illustrate the reason for this middle expansion, the development of the simulated freezing state of the sample was also shown in Figure 17. Then, we can see that the start

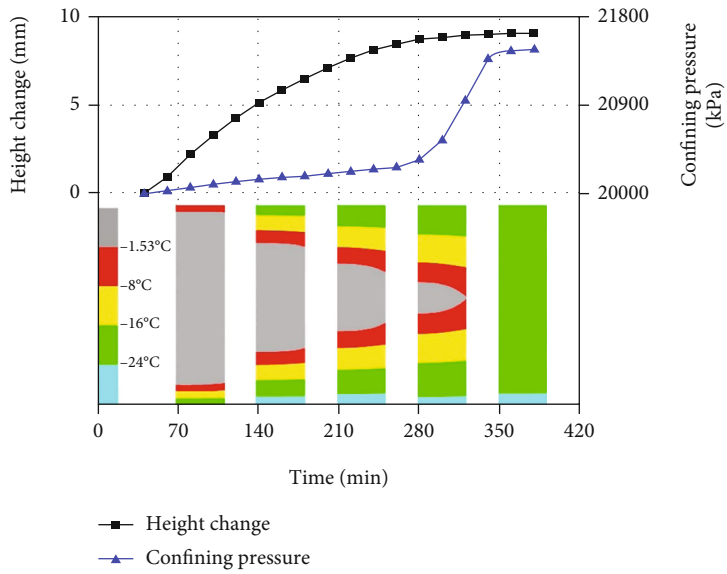

Figure 17: Changes in the simulated freezing state of the sample, the measured sample height, and the measured confining pressure over time under the condition that the mean temperature of the confining medium was controlled but the sample was frozen with two freezing fronts developing towards each other. The freezing state of the sample is shown through an axisymmetric plane, and the time corresponds to the symmetry axis (left border of the plane).

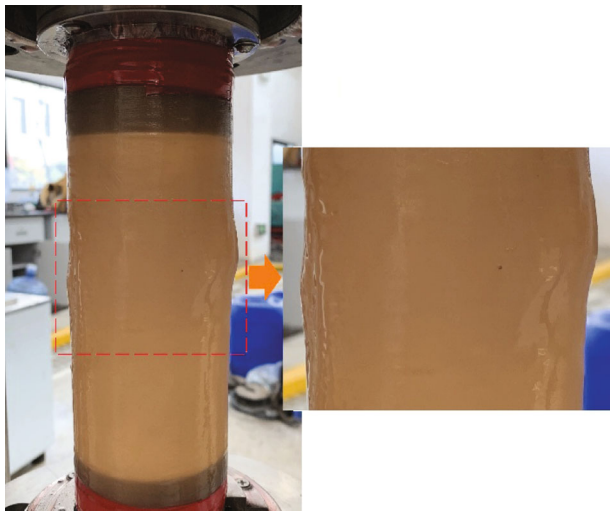

Figure 18: Ice sample frozen with two freezing fronts developing towards each other. The middle expansion is shown with double magnification.

time of the abnormal increase in the confining pressure was very close to the moment at which the two freezing fronts begin to merge, and after this merging, the sample height showed almost no further increase. This indicated that the merging of the two freezing fronts locked the sample height, preventing freezing expansion from continuing to occur along the height direction and causing the remaining freezing expansion to develop only in the radial direction, thereby compressing the confining medium; hence, the confining pressure abnormally increased, and the ice sample expanded in the middle. Therefore, the sample should be unidirectionally frozen to allow the freezing expansion to develop along the height direction throughout the whole freezing process.

7. Conclusions

A preparation technique for freezing pressurized water into a standard cylindrical ice sample in a triaxial cell was developed, in which the dimensional accuracy of the ice sample is guaranteed by the following measures:

(1) A cylindrical water sample with precise dimensions and strong sealing is fabricated using heat shrinkable tubing, sectional end caps, and an assembly cylinder, and a specially designed mounting device is used to maintain invariant relative positions between the upper and lower ends of the water sample during the insertion of the water sample into the triaxial cell

(2) During freezing, the quantity of the confining medium in the triaxial cell is locked by a pressure volume controller to restrict the radial deformation of the sample, and the pressure on the sample is controlled by the load frame, which is set to apply constant axial pressure. This ensures that freezing expansion will develop along the height direction through releasing the expansion pressure

(3) As the volume of the confining medium changes with temperature, the mean temperature of the confining medium should be controlled to vary $[(-0.25 - 0.073\,p_c) \pm 1.85]^{\circ}$C. This means that once the sample begins to freeze, the volume of the confining medium should be slightly decreased by changing the mean temperature by $(-0.25 - 0.073\,p_c)^{\circ}$C to allow the freezing expansion to develop to a small extent along the radial direction to compensate for the small radial shrinkage of the water sample caused by cooling and compression, then the mean temperature of the confining medium should remain constant

until the sample is completely frozen, and the controlling error should not exceed ±1.85°C

(4) The sample should be frozen by one freezing front developing in the bottom-up direction to ensure that the freezing expansion will develop in the height direction throughout the whole freezing process

(5) The control of the confining medium mean temperature and the sample unidirectional freezing can be realized by a numerical simulation in which the temperature constraints of the three freezing channel are adjusted

(6) The complete preparation procedures are as follows: first, the adjustment simulation of the temperature fields is carried out to determine the adjustments to the temperature constraints on the freezing channels; then, according to the simulation results, the temperature fields of the sample and the confining medium in the stages of triaxial cell precooling and precooled hydraulic oil injection and pressurization are controlled by the lateral freezing channel, and the upper and lower freezing channels are used to control the temperature fields during the freezing process

Data Availability

The data used to support the findings of this study are included within the article.

Conflicts of Interest

The authors declare that they have no conflicts of interest.

Acknowledgments

This work was supported by funding from the National Key Research and Development Program of China (Grant No. 2016YFC0600904).

References

[1] J. T. Chen, J. Zhao, S. Zhang, Y. Zhang, F. Yang, and M. Li, "An experimental and analytical research on the evolution of mining cracks in deep floor rock mass," *Pure and Applied Geophysics*, vol. 177, no. 11, pp. 5325–5348, 2020.

[2] B. Chen, S. Zhang, Y. Li, Z. Li, and H. Zhou, "Physical simulation study of crack propagation and instability information discrimination of rock-like materials with faults," *Arabian Journal of Geosciences*, vol. 13, no. 18, p. 966, 2020.

[3] D. K. Liu, Z. Gu, R. Liang et al., "Impacts of pore-throat system on fractal characterization of tight sandstones," *Geofluids*, vol. 2020, Article ID 4941501, 17 pages, 2020.

[4] T. Wang, H. Zhang, G. Q. Zhou, and X. Y. Liu, "Evaluation of variability characteristics of mechanical parameters of artificially frozen clay in deep alluvium," *Cold Regions Science and Technology*, vol. 171, p. 102978, 2020.

[5] Q. Yin, G. Ma, H. Jing et al., "Hydraulic properties of 3D rough-walled fractures during shearing: an experimental study," *Journal of Hydrology*, vol. 555, pp. 169–184, 2017.

[6] Q. Yin, H. Jing, G. Ma, H. Su, and R. Liu, "Investigating the roles of included angle and loading condition on the critical hydraulic gradient of real rock fracture networks," *Rock Mechanics and Rock Engineering*, vol. 51, no. 10, pp. 3167–3177, 2018.

[7] Y. Ji, G. Zhou, Y. Zhou, M. R. Hall, X. Zhao, and P. Q. Mo, "A separate-ice based solution for frost heaving-induced pressure during coupled thermal-hydro-mechanical processes in freezing soils," *Cold Regions Science and Technology*, vol. 147, pp. 22–33, 2018.

[8] J. Wang, Y. Zhang, Z. Qin, S. Song, and P. Lin, "Analysis method of water inrush for tunnels with damaged water-resisting rock mass based on finite element method-smooth particle hydrodynamics coupling," *Computers and Geotechnics*, vol. 126, p. 103725, 2020.

[9] J. P. Wang, W. M. Liu, and H. Wang, "Comparisons on ground freezing constructions in 1000 m depth mine shafts," *Mine Construction Technology*, vol. 38, no. 4, pp. 34–37, 2017.

[10] B. Zhang, W. H. Yang, and B. S. Wang, "Elastoplastic design theory for ultra-deep frozen wall considering large deformation features," *Chinese Journal of Geotechnical Engineering*, vol. 41, no. 7, pp. 1288–1295, 2019.

[11] R. L. Shan, Y. Bai, L. Song, and Y. Song, "Experimental study of blasting vibration and damage characteristics on frozen shaft wall," *Chinese Journal of Rock Mechanics and Engineering*, vol. S3, no. 34, pp. 3732–3741, 2015.

[12] R. Margesin, *Permafrost Soils*, Springer Science & Business Media, Heidelberg, Berlin, 2008.

[13] M. Ramos, A. Hasler, G. Vieira, C. Hauck, and S. Gruber, "Drilling and installation of boreholes for permafrost thermal monitoring on Livingston Island in the maritime Antarctic," *Permafrost & Periglacial Processes*, , pp. 57–64, 2009.

[14] D. Li, C. Zhang, G. Ding et al., "Fractional derivative-based creep constitutive model of deep artificial frozen soil," *Cold Regions Science and Technology*, vol. 170, p. 102942, 2020.

[15] D. Wang, W. Ma, X. Chang, and A. Wang, "Study on the resistance to deformation of artificially frozen soil in deep alluvium," *Cold Regions Science and Technology*, vol. 42, no. 3, pp. 194–200, 2005.

[16] Y. Yang, Y. Lai, and X. Chang, "Laboratory and theoretical investigations on the deformation and strength behaviors of artificial frozen soil," *Cold Regions Science and Technology*, vol. 64, no. 1, pp. 39–45, 2010.

[17] Y. Bai, R. Shan, Y. Ju et al., "Experimental study on the strength, deformation and crack evolution behaviour of red sandstone samples containing two ice-filled fissures under triaxial compression," *Cold Regions Science and Technology*, vol. 174, p. 103061, 2020.

[18] Y. Bai, R. Shan, Y. Ju, Y. Wu, P. Sun, and Z. Wang, "Study on the mechanical properties and damage constitutive model of frozen weakly cemented red sandstone," *Cold Regions Science and Technology*, vol. 171, p. 102980, 2020.

[19] R. L. Shan, Y. Bai, H. Dou, T. Han, and F. Yan, "Experimental study on the mechanical properties and damage evolution of red sandstone containing a single ice-filled flaw under triaxial compression," *Arabian Journal of Geosciences*, vol. 13, no. 14, 2020.

[20] M. J. Siegert, R. Kwok, C. Mayer, and B. Hubbard, "Water exchange between the subglacial Lake Vostok and the overlying ice sheet," *Nature*, vol. 403, no. 6770, pp. 643–646, 2000.

[21] V. Lukin and S. Bulat, "Vostok subglacial lake: details of Russian plans/activities for drilling and sampling," in *Geophysical Monograph Series*, American Geophysical Union, 2011.

[22] J. Jouzel, J. R. Petit, R. Souchez et al., "More than 200 meters of lake ice above subglacial Lake Vostok, Antarctica," *Science*, vol. 286, no. 5447, pp. 2138–2141, 1999.

[23] M. H. Carr, M. J. S. Belton, C. R. Chapman et al., "Evidence for a subsurface ocean on Europa," *Nature*, vol. 391, no. 6665, pp. 363–365, 1998.

[24] G. A. Kuehn, R. W. Lee, W. A. Nixon, and E. M. Schulson, "The structure and tensile behavior of first-year sea ice and laboratory-grown saline ice," *Journal of Offshore Mechanics and Arctic Engineering*, vol. 112, no. 4, pp. 357–363, 1990.

[25] T. R. Smith and E. M. Schulson, "The brittle compressive failure of fresh-water columnar ice under biaxial loading," *Acta Metallurgica et Materialia*, vol. 41, no. 1, pp. 153–163, 1993.

[26] W. F. Weeks and G. F. N. Cox, *Laboratory Preparation of Artificial Sea and Salt Ice*, Cold Regions Research and Engineering Laboratory, 1974.

[27] I. L. Meglis, R. E. Gagnon, and R. P. Young, "Microcracking during stress-relief of polycrystalline ice formed at high pressure," *Geophysical Research Letters*, vol. 22, no. 16, pp. 2207–2210, 1995.

[28] M. Arakawa and N. Maeno, "Mechanical strength of polycrystalline ice under uniaxial compression," *Cold Regions Science and Technology*, vol. 26, no. 3, pp. 215–229, 1997.

[29] R. E. Gagnon and P. H. Gammon, "Triaxial experiments on iceberg and glacier ice," *Journal of Glaciology*, vol. 41, no. 139, pp. 528–540, 1995.

[30] S. Y. Kim and K. Choi, "Standardization of laboratory experimental techniques with a cold room in Korea," in *Proceedings of the 18th IAHR International Symposium on Ice*, Sapporo, Japan, 2006.

[31] P. M. Melanson, I. L. Meglis, I. J. Jordaan, and B. M. Stone, "Microstructural change in ice: I. Constant-deformation-rate tests under triaxial stress conditions," *Journal of Glaciology*, vol. 45, no. 151, pp. 417–422, 1999.

[32] M. A. Rist and S. A. F. Murrell, "Ice triaxial deformation and fracture," *Journal of Glaciology*, vol. 40, no. 135, pp. 305–318, 1994.

[33] B. M. Stone, I. J. Jordaan, J. Xiao, and S. J. Jone, "Experiments on the damage process in ice under compressive states of stress," *Journal of Glaciology*, vol. 43, no. 143, pp. 11–25, 1997.

[34] G. A. Kuehn, E. M. Schulson, D. E. Jones, and J. Zhang, "The compressive strength of ice cubes of different sizes," *Journal of Offshore Mechanics and Arctic Engineering*, vol. 115, no. 2, pp. 142–148, 1993.

[35] I. Hawkes and M. Mellor, "Uniaxial testing in rock mechanics laboratories," *Engineering Geology*, vol. 4, no. 3, pp. 177–285, 1970.

[36] K. Mogi, *Experimental Rock Mechanics*, Taylor & Francis, 2006.

[37] M. S. Paterson and T. F. Wong, *Experimental Rock Deformation - the Brittle Field*, Springer, 2005.

[38] D. M. Cole, "Preparation of polycrystalline ice specimens for laboratory experiments," *Cold Regions Science and Technology*, vol. 1, no. 2, pp. 153–159, 1979.

[39] J. Schwarz, R. Frederking, V. Gavrillo et al., "Standardized testing methods for measuring mechanical properties of ice," *Cold Regions Science and Technology*, vol. 4, no. 3, pp. 245–253, 1981.

[40] R. Ulusay, *The ISRM Suggested Methods for Rock Characterization, Testing and Monitoring: 2007-2014*, Springer International Publishing, Switzerland, 2015.

[41] V. Petrenko and R. Whitworth, *Physics of Ice*, Oxford University Press, 2002.

[42] S. Timoshenk and S. W. Krieger, *Theory of Plates and Shells*, McGraw-Hill, 1959.

[43] P. R. Sammonds, S. A. F. Murrell, M. A. Rist, and D. Butler, "The design of a high-pressure low-temperature triaxial deformation cell for ice," *Cold Regions Science and Technology*, vol. 19, no. 2, pp. 177–188, 1991.

[44] B. D. Alkire and O. B. Andersland, "The effect of confining pressure on the mechanical properties of sand–ice materials," *Journal of Glaciology*, vol. 12, no. 66, pp. 469–481, 1973.

[45] Y. L. Chen, "Permeability evolution in granite under compressive stress condition," *Geotechnical and Geological Engineering*, vol. 36, no. 1, pp. 641–647, 2018.

[46] Q. Yin, R. Liu, H. Jing, H. Su, L. Yu, and L. He, "Experimental study of nonlinear flow behaviors through fractured rock samples after high-temperature exposure," *Rock Mechanics and Rock Engineering*, vol. 52, no. 9, pp. 2963–2983, 2019.

[47] J. W. Chen, H. Q. Hou, and W. J. Chen, "Study on deformation performance of PVC membrane materials under biaxial cyclic tensile loads," *Advanced Materials Research*, vol. 479-481, pp. 36–40, 2012.

[48] S. R. Chen, P. L. Kuai, and Q. L. Zhang, "Experimental research on mechanical properties of PVC membrane after artificial accelerated aging," *Structural Engineer*, vol. 29, no. 5, pp. 150–154, 2013.

[49] G. S. Kell, "Precise representation of volume properties of water at one atmosphere," *Journal of Chemical and Engineering Data*, vol. 12, no. 1, pp. 67–69, 1967.

[50] A. Bahadori and H. B. Vuthaluru, "Prediction of bulk modulus and volumetric expansion coefficient of water for leak tightness test of pipelines," *International Journal of Pressure Vessels and Piping*, vol. 86, no. 8, pp. 550–554, 2009.

[51] Y. Huang, G. J. Tang, and M. Zhu, "Large deformation analysis of elastic thin shells," *Engineering Mechanics*, vol. 19, no. 1, pp. 66–71, 2002.

[52] T. Makita, "Application of high pressure and thermophysical properties of water to biotechnology," *Fluid Phase Equilibria*, vol. 76, pp. 87–95, 1992.

[53] L. Otero, A. D. Molina-García, and P. D. Sanz, "Some interrelated thermophysical properties of liquid water and ice. I. A user-friendly modeling review for food high-pressure processing," *Critical Reviews in Food Science and Nutrition*, vol. 42, no. 4, pp. 339–352, 2002.

[54] D. Eisenberg and W. Kauzmann, *The Structure and Properties of Water*, Oxford University Pressure, London, 2005.

[55] W. Wagner, A. Saul, and A. Pruss, "International equations for the pressure along the melting and along the sublimation curve of ordinary water substance," *Journal of Physical and Chemical Reference Data*, vol. 23, no. 3, pp. 515–527, 1994.

[56] R. W. Blue, "The librational heat capacity of ice and of heavy ice," *Journal of Chemical Physics*, vol. 22, no. 2, pp. 280–283, 1954.

[57] G. A. Slack, "Thermal conductivity of ice," *Physical Review B*, vol. 22, no. 6, pp. 3065–3071, 1980.

[58] R. Gu and H. G. Stefan, "Year-round temperature simulation of cold climate lakes," *Cold Regions Science and Technology*, vol. 18, no. 2, pp. 147–160, 1990.

[59] M. L. V. Ramires, C. A. Nieto de Castro, Y. Nagasaka, A. Nagashima, M. J. Assael, and W. A. Wakeham, "Standard reference data for the thermal conductivity of water," *Journal of Physical and Chemical Reference Data*, vol. 24, no. 3, pp. 1377–1381, 1995.

[60] W. Cubberly, P. Unterweiser, D. Benjamin, C. Kirkpatrick, and K. Nieman, "Properties and selection: stainless steels, tool materials and special-purpose metals," in *Metals Handbook*, vol. 3, American Society for Metals, 1980.

[61] P. T. Tsilingiris, "Review and critical comparative evaluation of moist air thermophysical properties at the temperature range between 0 and 100°C for engineering calculations," *Renewable and Sustainable Energy Reviews*, vol. 83, pp. 50–63, 2018.